PHYSICAL REVIEW D **86,** 051105(R) (2012)

Improved limits on B^0 decays to invisible $(+\gamma)$ final states

J. P. Lees,[1] V. Poireau,[1] V. Tisserand,[1] J. Garra Tico,[2] E. Grauges,[2] A. Palano,[3a,3b] G. Eigen,[4] B. Stugu,[4] D. N. Brown,[5] L. T. Kerth,[5] Yu. G. Kolomensky,[5] G. Lynch,[5] H. Koch,[6] T. Schroeder,[6] D. J. Asgeirsson,[7] C. Hearty,[7] T. S. Mattison,[7] J. A. McKenna,[7] R. Y. So,[7] A. Khan,[8] V. E. Blinov,[9] A. R. Buzykaev,[9] V. P. Druzhinin,[9] V. B. Golubev,[9] E. A. Kravchenko,[9] A. P. Onuchin,[9] S. I. Serednyakov,[9] Yu. I. Skovpen,[9] E. P. Solodov,[9] K. Yu. Todyshev,[9] A. N. Yushkov,[9] M. Bondioli,[10] D. Kirkby,[10] A. J. Lankford,[10] M. Mandelkern,[10] H. Atmacan,[11] J. W. Gary,[11] F. Liu,[11] O. Long,[11] G. M. Vitug,[11] C. Campagnari,[12] T. M. Hong,[12] D. Kovalskyi,[12] J. D. Richman,[12] C. A. West,[12] A. M. Eisner,[13] J. Kroseberg,[13] W. S. Lockman,[13] A. J. Martinez,[13] B. A. Schumm,[13] A. Seiden,[13] D. S. Chao,[14] C. H. Cheng,[14] B. Echenard,[14] K. T. Flood,[14] D. G. Hitlin,[14] P. Ongmongkolkul,[14] F. C. Porter,[14] A. Y. Rakitin,[14] R. Andreassen,[15] Z. Huard,[15] B. T. Meadows,[15] M. D. Sokoloff,[15] L. Sun,[15] P. C. Bloom,[16] W. T. Ford,[16] A. Gaz,[16] U. Nauenberg,[16] J. G. Smith,[16] S. R. Wagner,[16] R. Ayad,[17,*] W. H. Toki,[17] B. Spaan,[18] K. R. Schubert,[19] R. Schwierz,[19] D. Bernard,[20] M. Verderi,[20] P. J. Clark,[21] S. Playfer,[21] D. Bettoni,[22a] C. Bozzi,[22a] R. Calabrese,[22a,22b] G. Cibinetto,[22a,22b] E. Fioravanti,[22a,22b] I. Garzia,[22a,22b] E. Luppi,[22a,22b] M. Munerato,[22a,22b] L. Piemontese,[22a] V. Santoro,[22a] R. Baldini-Ferroli,[23] A. Calcaterra,[23] R. de Sangro,[23] G. Finocchiaro,[23] P. Patteri,[23] I. M. Peruzzi,[23,†] M. Piccolo,[23] M. Rama,[23] A. Zallo,[23] R. Contri,[24a,24b] E. Guido,[24a,24b] M. Lo Vetere,[24a,24b] M. R. Monge,[24a,24b] S. Passaggio,[24a] C. Patrignani,[24a,24b] E. Robutti,[24a] B. Bhuyan,[25] V. Prasad,[25] C. L. Lee,[26] M. Morii,[26] A. J. Edwards,[27] A. Adametz,[28] U. Uwer,[28] H. M. Lacker,[29] T. Lueck,[29] P. D. Dauncey,[30] U. Mallik,[31] C. Chen,[32] J. Cochran,[32] W. T. Meyer,[32] S. Prell,[32] A. E. Rubin,[32] A. V. Gritsan,[33] Z. J. Guo,[33] N. Arnaud,[34] M. Davier,[34] D. Derkach,[34] G. Grosdidier,[34] F. Le Diberder,[34] A. M. Lutz,[34] B. Malaescu,[34] P. Roudeau,[34] M. H. Schune,[34] A. Stocchi,[34] G. Wormser,[34] D. J. Lange,[35] D. M. Wright,[35] C. A. Chavez,[36] J. P. Coleman,[36] J. R. Fry,[36] E. Gabathuler,[36] D. E. Hutchcroft,[36] D. J. Payne,[36] C. Touramanis,[36] A. J. Bevan,[37] F. Di Lodovico,[37] R. Sacco,[37] M. Sigamani,[37] G. Cowan,[38] D. N. Brown,[39] C. L. Davis,[39] A. G. Denig,[40] M. Fritsch,[40] W. Gradl,[40] K. Griessinger,[40] A. Hafner,[40] E. Prencipe,[40] R. J. Barlow,[41,‡] G. Jackson,[41] G. D. Lafferty,[41] E. Behn,[42] R. Cenci,[42] B. Hamilton,[42] A. Jawahery,[42] D. A. Roberts,[42] C. Dallapiccola,[43] R. Cowan,[44] D. Dujmic,[44] G. Sciolla,[44] R. Cheaib,[45] D. Lindemann,[45] P. M. Patel,[45] S. H. Robertson,[45] P. Biassoni,[46a,46b] N. Neri,[46a] F. Palombo,[46a,46b] S. Stracka,[46a,46b] L. Cremaldi,[47] R. Godang,[47,§] R. Kroeger,[47] P. Sonnek,[47] D. J. Summers,[47] X. Nguyen,[48] M. Simard,[48] P. Taras,[48] G. De Nardo,[49a,49b] D. Monorchio,[49a,49b] G. Onorato,[49a,49b] C. Sciacca,[49a,49b] M. Martinelli,[50] G. Raven,[50] C. P. Jessop,[51] J. M. LoSecco,[51] W. F. Wang,[51] K. Honscheid,[52] R. Kass,[52] J. Brau,[53] R. Frey,[53] N. B. Sinev,[53] D. Strom,[53] E. Torrence,[53] E. Feltresi,[54a,54b] N. Gagliardi,[54a,54b] M. Margoni,[54a,54b] M. Morandin,[54a] M. Posocco,[54a] M. Rotondo,[54a] G. Simi,[54a] F. Simonetto,[54a,54b] R. Stroili,[54a,54b] S. Akar,[55] E. Ben-Haim,[55] M. Bomben,[55] G. R. Bonneaud,[55] H. Briand,[55] G. Calderini,[55] J. Chauveau,[55] O. Hamon,[55] Ph. Leruste,[55] G. Marchiori,[55] J. Ocariz,[55] S. Sitt,[55] M. Biasini,[56a,56b] R. Covarelli,[56a,56b,‖] E. Manoni,[56a,56b] S. Pacetti,[56a,56b] A. Rossi,[56a,56b] C. Angelini,[57a,57b] G. Batignani,[57a,57b] S. Bettarini,[57a,57b] M. Carpinelli,[57a,57b,¶] G. Casarosa,[57a,57b] A. Cervelli,[57a,57b] F. Forti,[57a,57b] M. A. Giorgi,[57a,57b] A. Lusiani,[57a,57c] B. Oberhof,[57a,57b] E. Paoloni,[57a,57b] A. Perez,[57a] G. Rizzo,[57a,57b] J. J. Walsh,[57a] D. Lopes Pegna,[58] J. Olsen,[58] A. J. S. Smith,[58] A. V. Telnov,[58] F. Anulli,[59a] R. Faccini,[59a,59b] F. Ferrarotto,[59a] F. Ferroni,[59a,59b] M. Gaspero,[59a,59b] L. Li Gioi,[59a] M. A. Mazzoni,[59a] G. Piredda,[59a] C. Bünger,[60] O. Grünberg,[60] T. Hartmann,[60] T. Leddig,[60] H. Schröder,[60,**] C. Voss,[60] R. Waldi,[60] T. Adye,[61] E. O. Olaiya,[61] F. F. Wilson,[61] S. Emery,[62] G. Hamel de Monchenault,[62] G. Vasseur,[62] Ch. Yèche,[62] D. Aston,[63] D. J. Bard,[63] R. Bartoldus,[63] J. F. Benitez,[63] C. Cartaro,[63] M. R. Convery,[63] J. Dorfan,[63] G. P. Dubois-Felsmann,[63] W. Dunwoodie,[63] M. Ebert,[63] R. C. Field,[63] M. Franco Sevilla,[63] B. G. Fulsom,[63] A. M. Gabareen,[63] M. T. Graham,[63] P. Grenier,[63] C. Hast,[63] W. R. Innes,[63] M. H. Kelsey,[63] P. Kim,[63] M. L. Kocian,[63] D. W. G. S. Leith,[63] P. Lewis,[63] B. Lindquist,[63] S. Luitz,[63] V. Luth,[63] H. L. Lynch,[63] D. B. MacFarlane,[63] D. R. Muller,[63] H. Neal,[63] S. Nelson,[63] M. Perl,[63] T. Pulliam,[63] B. N. Ratcliff,[63] A. Roodman,[63] A. A. Salnikov,[63] R. H. Schindler,[63] A. Snyder,[63] D. Su,[63] M. K. Sullivan,[63] J. Va'vra,[63] A. P. Wagner,[63] W. J. Wisniewski,[63] M. Wittgen,[63] D. H. Wright,[63] H. W. Wulsin,[63] C. C. Young,[63] V. Ziegler,[63] W. Park,[64] M. V. Purohit,[64] R. M. White,[64] J. R. Wilson,[64] A. Randle-Conde,[65] S. J. Sekula,[65] M. Bellis,[66] P. R. Burchat,[66] T. S. Miyashita,[66] E. M. T. Puccio,[66] M. S. Alam,[67] J. A. Ernst,[67] R. Gorodeisky,[67] N. Guttman,[67] D. R. Peimer,[68] A. Soffer,[68] P. Lund,[68] S. M. Spanier,[69] J. L. Ritchie,[69] A. M. Ruland,[70] R. F. Schwitters,[70] B. C. Wray,[70] J. M. Izen,[71] X. C. Lou,[71] F. Bianchi,[72a,72b] D. Gamba,[72a,72b] S. Zambito,[72a,72b] L. Lanceri,[73a,73b] L. Vitale,[73a,73b] F. Martinez-Vidal,[74] A. Oyanguren,[74] H. Ahmed,[75] J. Albert,[75] Sw. Banerjee,[75] F. U. Bernlochner,[75] H. H. F. Choi,[75] G. J. King,[75] R. Kowalewski,[75] M. J. Lewczuk,[75] I. M. Nugent,[75] J. M. Roney,[75] R. J. Sobie,[75] N. Tasneem,[75] T. J. Gershon,[76] P. F. Harrison,[76] T. E. Latham,[76] H. R. Band,[77] S. Dasu,[77] Y. Pan,[77] R. Prepost,[77] and S. L. Wu[77]

(The *BABAR* Collaboration)

[1]*Laboratoire d'Annecy-le-Vieux de Physique des Particules (LAPP), Université de Savoie, CNRS/IN2P3, F-74941 Annecy-Le-Vieux, France*
[2]*Universitat de Barcelona, Facultat de Fisica, Departament ECM, E-08028 Barcelona, Spain*
[3a]*INFN Sezione di Bari, I-70126 Bari, Italy*
[3b]*Dipartimento di Fisica, Università di Bari, I-70126 Bari, Italy*
[4]*University of Bergen, Institute of Physics, N-5007 Bergen, Norway*
[5]*Lawrence Berkeley National Laboratory and University of California, Berkeley, California 94720, USA*
[6]*Ruhr Universität Bochum, Institut für Experimentalphysik 1, D-44780 Bochum, Germany*
[7]*University of British Columbia, Vancouver, British Columbia, Canada V6T 1Z1*
[8]*Brunel University, Uxbridge, Middlesex UB8 3PH, United Kingdom*
[9]*Budker Institute of Nuclear Physics, Novosibirsk 630090, Russia*
[10]*University of California at Irvine, Irvine, California 92697, USA*
[11]*University of California at Riverside, Riverside, California 92521, USA*
[12]*University of California at Santa Barbara, Santa Barbara, California 93106, USA*
[13]*University of California at Santa Cruz, Institute for Particle Physics, Santa Cruz, California 95064, USA*
[14]*California Institute of Technology, Pasadena, California 91125, USA*
[15]*University of Cincinnati, Cincinnati, Ohio 45221, USA*
[16]*University of Colorado, Boulder, Colorado 80309, USA*
[17]*Colorado State University, Fort Collins, Colorado 80523, USA*
[18]*Technische Universität Dortmund, Fakultät Physik, D-44221 Dortmund, Germany*
[19]*Technische Universität Dresden, Institut für Kern- und Teilchenphysik, D-01062 Dresden, Germany*
[20]*Laboratoire Leprince-Ringuet, Ecole Polytechnique, CNRS/IN2P3, F-91128 Palaiseau, France*
[21]*University of Edinburgh, Edinburgh EH9 3JZ, United Kingdom*
[22a]*INFN Sezione di Ferrara, I-44100 Ferrara, Italy*
[22b]*Dipartimento di Fisica, Università di Ferrara, I-44100 Ferrara, Italy*
[23]*INFN Laboratori Nazionali di Frascati, I-00044 Frascati, Italy*
[24a]*INFN Sezione di Genova, I-16146 Genova, Italy*
[24b]*Dipartimento di Fisica, Università di Genova, I-16146 Genova, Italy*
[25]*Indian Institute of Technology Guwahati, Guwahati, Assam, 781 039, India*
[26]*Harvard University, Cambridge, Massachusetts 02138, USA*
[27]*Harvey Mudd College, Claremont, California 91711*
[28]*Universität Heidelberg, Physikalisches Institut, Philosophenweg 12, D-69120 Heidelberg, Germany*
[29]*Humboldt-Universität zu Berlin, Institut für Physik, Newtonstr. 15, D-12489 Berlin, Germany*
[30]*Imperial College London, London, SW7 2AZ, United Kingdom*
[31]*University of Iowa, Iowa City, Iowa 52242, USA*
[32]*Iowa State University, Ames, Iowa 50011-3160, USA*
[33]*Johns Hopkins University, Baltimore, Maryland 21218, USA*
[34]*Laboratoire de l'Accélérateur Linéaire, IN2P3/CNRS et Université Paris-Sud 11, Centre Scientifique d'Orsay, B. P. 34, F-91898 Orsay Cedex, France*
[35]*Lawrence Livermore National Laboratory, Livermore, California 94550, USA*
[36]*University of Liverpool, Liverpool L69 7ZE, United Kingdom*
[37]*Queen Mary, University of London, London, E1 4NS, United Kingdom*
[38]*University of London, Royal Holloway and Bedford New College, Egham, Surrey TW20 0EX, United Kingdom*
[39]*University of Louisville, Louisville, Kentucky 40292, USA*
[40]*Johannes Gutenberg-Universität Mainz, Institut für Kernphysik, D-55099 Mainz, Germany*
[41]*University of Manchester, Manchester M13 9PL, United Kingdom*
[42]*University of Maryland, College Park, Maryland 20742, USA*
[43]*University of Massachusetts, Amherst, Massachusetts 01003, USA*
[44]*Massachusetts Institute of Technology, Laboratory for Nuclear Science, Cambridge, Massachusetts 02139, USA*
[45]*McGill University, Montréal, Québec, Canada H3A 2T8*
[46a]*INFN Sezione di Milano, I-20133 Milano, Italy*
[46b]*Dipartimento di Fisica, Università di Milano, I-20133 Milano, Italy*
[47]*University of Mississippi, University, Mississippi 38677, USA*
[48]*Université de Montréal, Physique des Particules, Montréal, Québec, Canada H3C 3J7*
[49a]*INFN Sezione di Napoli, I-80126 Napoli, Italy*
[49b]*Dipartimento di Scienze Fisiche, Università di Napoli Federico II, I-80126 Napoli, Italy*
[50]*NIKHEF, National Institute for Nuclear Physics and High Energy Physics, NL-1009 DB Amsterdam, The Netherlands*

[51]*University of Notre Dame, Notre Dame, Indiana 46556, USA*
[52]*Ohio State University, Columbus, Ohio 43210, USA*
[53]*University of Oregon, Eugene, Oregon 97403, USA*
[54a]*INFN Sezione di Padova, I-35131 Padova, Italy*
[54b]*Dipartimento di Fisica, Università di Padova, I-35131 Padova, Italy*
[55]*Laboratoire de Physique Nucléaire et de Hautes Energies, IN2P3/CNRS, Université Pierre et Marie Curie-Paris6, Université Denis Diderot-Paris7, F-75252 Paris, France*
[56a]*INFN Sezione di Perugia, I-06100 Perugia, Italy*
[56b]*Dipartimento di Fisica, Università di Perugia, I-06100 Perugia, Italy*
[57a]*INFN Sezione di Pisa, I-56127 Pisa, Italy*
[57b]*Dipartimento di Fisica, Università di Pisa, I-56127 Pisa, Italy*
[57c]*Scuola Normale Superiore di Pisa, I-56127 Pisa, Italy*
[58]*Princeton University, Princeton, New Jersey 08544, USA*
[59a]*INFN Sezione di Roma, I-00185 Roma, Italy*
[59b]*Dipartimento di Fisica, Università di Roma La Sapienza, I-00185 Roma, Italy*
[60]*Universität Rostock, D-18051 Rostock, Germany*
[61]*Rutherford Appleton Laboratory, Chilton, Didcot, Oxon, OX11 0QX, United Kingdom*
[62]*CEA, Irfu, SPP, Centre de Saclay, F-91191 Gif-sur-Yvette, France*
[63]*SLAC National Accelerator Laboratory, Stanford, California 94309 USA*
[64]*University of South Carolina, Columbia, South Carolina 29208, USA*
[65]*Southern Methodist University, Dallas, Texas 75275, USA*
[66]*Stanford University, Stanford, California 94305-4060, USA*
[67]*State University of New York, Albany, New York 12222, USA*
[68]*Tel Aviv University, School of Physics and Astronomy, Tel Aviv, 69978, Israel*
[69]*University of Tennessee, Knoxville, Tennessee 37996, USA*
[70]*University of Texas at Austin, Austin, Texas 78712, USA*
[71]*University of Texas at Dallas, Richardson, Texas 75083, USA*
[72a]*INFN Sezione di Torino, I-10125 Torino, Italy*
[72b]*Dipartimento di Fisica Sperimentale, Università di Torino, I-10125 Torino, Italy*
[73a]*INFN Sezione di Trieste, I-34127 Trieste, Italy*
[73b]*Dipartimento di Fisica, Università di Trieste, I-34127 Trieste, Italy*
[74]*IFIC, Universitat de Valencia-CSIC, E-46071 Valencia, Spain*
[75]*University of Victoria, Victoria, British Columbia, Canada V8W 3P6*
[76]*Department of Physics, University of Warwick, Coventry CV4 7AL, United Kingdom*
[77]*University of Wisconsin, Madison, Wisconsin 53706, USA*

(Received 13 June 2012; published 27 September 2012)

We establish improved upper limits on branching fractions for B^0 decays to final states where the decay products are purely invisible (i.e., no observable final state particles) and for final states where the only visible product is a photon. Within the Standard Model, these decays have branching fractions that are below the current experimental sensitivity, but various models of physics beyond the Standard Model predict significant contributions for these channels. Using 471×10^6 $B\bar{B}$ pairs collected at the $\Upsilon(4S)$ resonance by the *BABAR* experiment at the PEP-II e^+e^- storage ring at the SLAC National Accelerator Laboratory, we establish upper limits at the 90% confidence level of 2.4×10^{-5} for the branching fraction of $B^0 \to$ invisible and 1.7×10^{-5} for the branching fraction of $B^0 \to$ invisible + γ.

DOI: 10.1103/PhysRevD.86.051105 PACS numbers: 13.20.He, 12.15.Ji, 12.60.Jv

This paper presents updated limits on "disappearance decays" of B^0 mesons [1], where the B^0 decay contains no observable final state particles, or such "invisible" decay products plus a single photon. We define invisible decay products here to be electrically neutral particles that do not generate a signal in the electromagnetic calorimeter. These results represent an improvement over the previous limits on these decays, which were based on 19% of the present data sample [2].

The rate for invisible B decays is negligibly small within the Standard Model (SM) of particle physics but can be

*Now at the University of Tabuk, Tabuk 71491, Saudi Arabia.
†Also with Università di Perugia, Dipartimento di Fisica, Perugia, Italy.
‡Now at the University of Huddersfield, Huddersfield HD1 3DH, UK.
§Now at University of South Alabama, Mobile, AL 36688, USA.
‖Now at University of Rochester, Rochester, NY, 14627, USA.
¶Also with Università di Sassari, Sassari, Italy.
**Deceased.

larger in several models of new physics. The SM decay $B^0 \to \nu\bar{\nu}$, which would give such an invisible experimental signature, is strongly helicity suppressed by a factor of order $(m_\nu/m_{B^0})^2$ [3], and the resulting branching fraction is necessarily well below the range of present experimental observability. The SM expectation for the $B^0 \to \nu\bar{\nu}\gamma$ branching fraction is predicted to be of order 10^{-9}, with very little uncertainty from hadronic interactions [4]. An experimental observation of an invisible $(+\gamma)$ decay of a B^0 with current experimental sensitivity would thus be a clear sign of physics beyond the SM.

A phenomenological model motivated by the observation of an anomalous number of dimuon events by the NuTeV experiment [5] allows for an invisible B^0 decay to a $\bar{\nu}\chi_1^0$ final state, where χ_1^0 is a neutralino, with a branching fraction in the 10^{-7} to 10^{-6} range [6]. Also, models with large extra dimensions, which would provide a possible solution to the hierarchy problem, can have the effect of producing significant, although small, rates for invisible B^0 decays [7–9].

The data used in this analysis were collected with the *BABAR* detector at the PEP-II e^+e^- collider at SLAC. The data sample corresponds to a luminosity of 424 fb^{-1} accumulated at the $\Upsilon(4S)$ resonance and contains $(471 \pm 3) \times 10^6$ $B\bar{B}$ pair events. For background studies we also used 45 fb^{-1} collected at a center-of-mass (CM) energy about 40 MeV below $B\bar{B}$ threshold (off peak).

A detailed description of the *BABAR* detector is presented in Ref. [10]. Charged particle momenta are measured in a tracking system consisting of a five-layer double-sided silicon vertex tracker (SVT) and a 40-layer hexagonal-cell wire drift chamber (DCH). The SVT and DCH operate within a 1.5 T solenoidal field and have a combined solid angle coverage in the CM frame of 90.5%. Photons and long-lived neutral hadrons are detected and their energies are measured in a CsI(Tl) electromagnetic calorimeter (EMC), which has a solid angle coverage in the CM frame of 90.9%. Muons are identified in the instrumented flux return. A detector of internally reflected Cherenkov light (DIRC) is used for identification of charged kaons and pions. A GEANT4 [11] based Monte Carlo (MC) simulation of the *BABAR* detector response is used to optimize the signal selection criteria and evaluate the signal detection efficiency.

The detection of invisible B decays uses the fact that B mesons are created in pairs, due to flavor conservation in e^+e^- interactions. If one B is reconstructed in an event, one can thus infer that another B has been produced. We reconstruct events in which a B^0 decays to $D^{(*)-}\ell^+\nu$ (referred to as the "tag side"), then look for consistency with an invisible decay or a decay to a single photon of the other neutral B (referred to as the "signal side"). The choice of reconstructing semileptonic B^0 decays on the tag side, with respect to fully reconstructed B^0 final states, is motivated by a higher reconstruction efficiency. A disadvantage is the presence of the invisible neutrino, which prevents the exploitation of kinematic variables such as the reconstructed B^0 mass. However, the background contamination is mitigated by the presence of a high momentum lepton.

We reconstruct D^{*-} mesons in the final states $\bar{D}^0\pi^-$ or $D^-\pi^0$, with $\bar{D}^0$ decays to $K^+\pi^-$, $K^+\pi^-\pi^0$, or $K^+\pi^-\pi^+\pi^-$, and D^- decays to $K^+\pi^-\pi^-$ or $K^0_S\pi^-$. We identify K^+ candidates using Cherenkov light information from the DIRC and energy-loss information ($\mathrm{d}E/\mathrm{d}x$) from the DCH and SVT. The K^0_S mesons are reconstructed in the decay mode $K^0_S \to \pi^+\pi^-$, where the π^+ π^- invariant mass lies in a ± 25 MeV/c^2 window around the nominal Particle Data Group (PDG) K^0_S mass [12]. The π^0 candidates are composed of pairs of photons observed in the EMC. Each photon must have a reconstructed energy above 30 MeV in the laboratory frame, and the sum of their energies must be greater than 200 MeV. The π^0 candidates must have an invariant mass between 115 and 150 MeV/c^2. A mass-constrained fit is imposed on π^0 candidates in order to improve the resolution on the reconstructed invariant mass of the parent D meson.

Kaon and pion candidates are then combined to reconstruct $D^{(*)}$ mesons. These are required to have an invariant mass within 60 MeV/c^2 of their nominal PDG mass, except for $\bar{D}^0$ decays with a π^0 daughter, which must be within 100 MeV/c^2 of the nominal $\bar{D}^0$ mass. Mass-constrained fits are applied to $\bar{D}^0$ and D^- candidates in order to improve the measurement of the momentum of each D. The difference in reconstructed mass between D^{*-} decay candidates and their D daughters must be less than 175 MeV/c^2 and greater than 137 MeV/c^2. All $D^{(*)-}$ candidates must have a total momentum between 0.5 and 2.5 GeV/c in the CM frame.

Tracks selected as lepton candidates must pass either electron or muon selection criteria. We identify electron candidates using energy and cluster shape information from the EMC, and Cherenkov angle information from the DIRC. Muon candidates are identified using information from the instrumented flux return and EMC. Both electrons and muons must also have a momentum of at least 0.8 GeV/c in the laboratory frame, and a minimum of 20 DCH measurements.

To further select $B^0 \to D^{(*)-}\ell^+\nu$ candidates, we require a $D^{(*)-}$ candidate and a lepton candidate to be consistent with production at a common point in space. The decay vertex is reconstructed from a kinematic fit to all the candidate daughters, and a minimum χ^2 vertex probability of 0.001 is required. We then calculate the cosine of the angle between the $D^{(*)-}\ell^+$ and the hypothesized B^0 candidate in the CM frame, under the assumption that the only particle missing is a neutrino:

$$\cos\theta_{B,D^{(*)-}\ell^+} = \frac{2E_B E_{D^{(*)-}\ell^+} - m_B^2 - m^2_{D^{(*)-}\ell^+}}{2|\vec{p}_B||\vec{p}_{D^{(*)-}\ell^+}|}. \quad (1)$$

The energy in the CM frame $E_{D^{(*)-}\ell^+}$ and mass $m_{D^{(*)-}\ell^+}$ of the $D^{(*)-}\ell^+$ combination are determined from reconstructed momentum information, and m_B is the nominal B^0 mass [12]. The B^0 momentum $|\vec{p}_B|$ and energy E_B in the CM frame are determined from beam parameters. If our assumption that there is only one missing particle, a neutrino, in the B^0 decays is incorrect, $\cos\theta_{B,D^{(*)-}\ell^+}$ can fall outside the region $[-1, 1]$. We require the $D^{(*)-}\ell^+$ combination to satisfy $-5.5 < \cos\theta_{B,D^{(*)-}\ell^+} < 1.5$. The selected region allows for nonphysical $\cos\theta_{B,D^{(*)-}\ell^+}$ values, accounting for detector energy and momentum resolution. Moreover the asymmetric cut admits higher D^* mass states where additional decay products are lost. In the rest of the analysis such products are not associated with the tag side decay chain but are considered as extra particles in the event. When more than one $B^0 \to D^{(*)-}\ell^+\nu$ candidate is reconstructed in an event, the one with the highest vertex probability is taken.

We consider events with no charged tracks besides those from the $B^0 \to D^{(*)-}\ell^+\nu$ candidate. In order to reject background events where one charged or neutral particle is lost along the beam pipe, the cosine of the polar angle of the missing momentum in the CM frame ($\cos\theta^*_{\rm miss}$) is required to lie in the $[-0.9, 0.9]$ range. The missing 4-momentum due to unreconstructed particles is defined as the difference between the $\Upsilon(4S)$ and the reconstructed tag side 4-momentum. In the $B^0 \to$ invisible + γ channel the signal-side photon 4-momentum is also subtracted from the $\Upsilon(4S)$ one.

For the $B^0 \to$ invisible decay, in events where the D meson on the tag side decays into $K^-\pi^+\pi^-$, two additional selection criteria are applied. The first concerns the sum of the cosine of the angles between the kaon and two pions, $\cos\theta_{K\pi_1} + \cos\theta_{K\pi_2} > -0.8$, while the second concerns the sum of the cosine of the angles between the lepton and the pions, $\cos\theta_{\ell\pi_1} + \cos\theta_{\ell\pi_2} < 0.8$. The main effect of this selection is the reduction of the background from misreconstructed $e^+e^- \to \tau^+\tau^-$ events.

To reconstruct $B^0 \to$ invisible + γ events, one remaining photon candidate with energy greater than 1.2 GeV in the CM frame is also required. If the detected photon has an energy smaller than 1.2 GeV in the CM frame, the event falls in the $B^0 \to$ invisible category and the neutral candidate is considered as an extra photon in the event. The choice of this cut generates a cross-feed between the two channels; MC simulation studies show that this has a negligible effect on the final result.

An artificial neural network (NN) is used to provide further discrimination between signal and background events. We use the TMVA software package [13] and its multilayer perception implementation of a NN. The architecture of the NN is composed of one input layer and one hidden layer. These layers have V and $2V$ nodes, respectively, where V is the number of the input variables. Samples that represent the signal and background components are given as input to the NN; one half of each of these samples is used for the training while the other half is used as test. Once the NN has been trained, the output distributions for training and test samples are compared in order to check the presence of overtraining problems. For the signal sample, MC simulation in which a generic semileptonic B decay is generated and reconstructed is used. Weighted off-peak data (composed of $e^+e^- \to c\bar{c}$, $u\bar{u}$, $s\bar{s}$, and $\tau^+\tau^-$ events, denoted as continuum background) and MC simulated $B\bar{B}$ events are used to describe the background contamination. Off-peak data are used to model continuum background, as the MC was found to incorrectly reproduce the cross section of two-photon fusion events, such as $e^+e^- \to e^+e^-\gamma\gamma \to e^+e^-q\bar{q}/\tau^+\tau^-$. These events typically have decay products directed along the beam lines, and thus outside the detector acceptance.

The variables used as input for the NN, common to the $B^0 \to$ invisible and $B^0 \to$ invisible + γ analyses, are (1) $\cos\theta_{B,D^{(*)-}\ell^+}$; (2) the cosine of the angle in the CM frame between the thrust axis (the axis along which the total longitudinal momentum of the event is maximized) and the $D^{(*)-}\ell^+$ pair momentum direction; and (3) the lepton momentum in the CM frame. In the $B^0 \to$ invisible analysis, we additionally use (1′) $M^{\rm tag}_{\rm miss}$ [defined as the invariant mass of the event after the $D^{(*)-}\ell^+$ pair is subtracted]; (2′) the B meson vertex fit probability; (3′) the ratio between the first and the zeroth order L momenta in the CM frame:

$$L_i = \sum p\cos^i\theta, \tag{2}$$

where the sum is over extra tracks and neutrals and θ is computed with respect to the thrust axis; (4′) the transverse momentum of the $D^-\ell^+$ pair in the CM frame; (5′) the minimum invariant mass of any two charged tracks in the event; and (6′) the minimum invariant mass of any three charged tracks in the event. Variables (4′)–(6′) enter the NN only in the case of a reconstructed $B^0 \to D^-\ell^+\nu$ decay on the tag side. In the $B^0 \to$ invisible + γ analysis, we additionally use (1″) the energy of the photon on the signal side evaluated in the laboratory frame and (2″) $M^{\rm tag}_{\rm miss}$ (for $B^0 \to D^-\ell^+\nu$ reconstructed events only).

The selection on the output of the NN is optimized by minimizing the expected upper limit on the branching fraction, defined by a Bayesian approach as detailed later in this paper, under the hypothesis of observing zero signal events. This optimization is performed by using $B\bar{B}$ MC simulation and weighted off-peak data samples for the background estimation and the signal MC sample for the selection efficiency. In Fig. 1, the output of the NN for simulated $B^0 \to$ invisible with a D meson on the tag side and the corresponding signal region are shown.

After the NN selection, the D meson invariant mass (m_D) and the difference between the reconstructed D^* invariant mass and the PDG D^0 mass (Δm) are used to

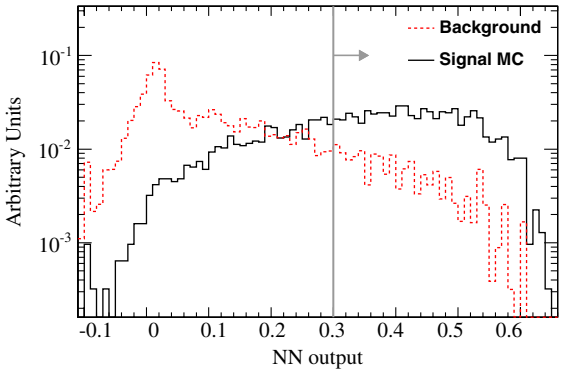

FIG. 1 (color online). Distributions of the NN output for simulated $B^0 \to$ invisible events with a D meson on the tag side. The black solid line is the signal while the red dashed line is the background. The solid gray vertical line defines the NN output signal region.

define a signal region (SR) and a side band region (SB) for the D tag and D^* tag samples, respectively. The SR is defined as a ± 15 MeV$/c^2$ window around the PDG value for m_D for the $B^0 \to D^- \ell^+ \nu$ sample, and as $0.139 < \Delta m < 0.148$ GeV$/c^2$ for the $B^0 \to D^{*-} \ell^+ \nu$ sample. The excluded regions are used as the SB region.

The total energy in the EMC computed in the CM frame and not associated with neutral particles or charged tracks used in the $D^{(*)-} \ell^+$ reconstruction is denoted as $E_{\rm extra}$. For $B^0 \to$ invisible $+ \gamma$, the energy of the highest-energy photon remaining in the event (the signal photon candidate) is also removed from the $E_{\rm extra}$ computation. The $E_{\rm extra}$ signal region is defined by imposing an upper bound at 1.2 GeV.

In both $B^0 \to$ invisible and $B^0 \to$ invisible $+ \gamma$ samples, this variable is strongly peaked near zero for signal, whereas for the background the distribution increases uniformly in the chosen signal region. Background events can, however, populate the low $E_{\rm extra}$ region, when charged or neutral particles from the event are either outside the fiducial volume of the detector or are unreconstructed due to detector inefficiencies. Contributions from misreconstructed π^0 decays usually populate the high $E_{\rm extra}$ region.

Using detailed Monte Carlo simulations of $B^0 \to$ invisible and $B^0 \to$ invisible $+ \gamma$ events, we determine our signal efficiency to be $(17.8 \pm 0.2) \times 10^{-4}$ for $B^0 \to$ invisible and $(16.0 \pm 0.2) \times 10^{-4}$ for $B^0 \to$ invisible $+ \gamma$, where the uncertainties are statistical. These efficiencies are enhanced by a factor 8.5% and 11%, respectively, with respect to the previous analysis [2]. The background selection efficiencies (evaluated in $B\bar{B}$ MC plus off-peak data) are 4.16×10^{-8} and 1.32×10^{-9} for the invisible and invisible $+ \gamma$ decay, respectively. These can be compared with the background selection efficiencies in the previous analysis, which were 2.79×10^{-7} and 4.96×10^{-8}, respectively.

We construct probability density functions (PDFs) for the $E_{\rm extra}$ distribution for signal ($\mathcal{P}_{\rm sig}$) and background ($\mathcal{P}_{\rm bkg}$) using detailed MC simulation for signal and data from the m_D and Δm sidebands for background. The two PDFs are combined into an extended maximum likelihood function $\mathcal{L}$, defined as a function of the free parameters $N_{\rm sig}$ and $N_{\rm bkg}$, the number of signal and background events, respectively:

$$\mathcal{L}(N_{\rm sig}, N_{\rm bkg}) = \frac{[(1-z_{\rm sig})N_{\rm sig} + (1-z_{\rm bkg})N_{\rm bkg}]^{N_1}}{N_1!} e^{-[(1-z_{\rm sig})N_{\rm sig} + (1-z_{\rm bkg})N_{\rm bkg}]} \prod_{i=1}^{N_1} \Big[\mathcal{P}_{\rm sig}(E_{{\rm extra},i}|\vec{p}_{\rm sig}) \frac{(1-z_{\rm sig})N_{\rm sig}}{N_1} + \mathcal{P}_{\rm bkg}(E_{\rm extra}, i|\vec{p}_{\rm bkg}) \frac{(1-z_{\rm bkg})N_{\rm bkg}}{N_1} \Big] \frac{(z_{\rm sig}N_{\rm sig} + z_{\rm bkg}N_{\rm bkg})^{N_0}}{N_0!} e^{-(z_{\rm sig}N_{\rm sig} + z_{\rm bkg}N_{\rm bkg})}. \quad (3)$$

The photon reconstruction has a detection lower energy bound of 30 MeV, and as a consequence, the $E_{\rm extra}$ distribution is not continuous. To account for this effect, the likelihood in Eq. (3) is composed of two distinct parts, one for $E_{\rm extra} > 30$ MeV and one for $E_{\rm extra} = 0$ MeV. In the likelihood function, $z_{\rm sig}$ and $z_{\rm bkg}$ are the fractions of events with $E_{\rm extra} = 0$ MeV for signal and background, respectively, and $\vec{p}_{\rm sig}$ and $\vec{p}_{\rm bkg}$ are the vectors of parameters describing the signal and background PDFs, a kernel-based PDF [14], and a second-order polynomial, respectively. The fixed parameters N_0, N_1, and $E_{{\rm extra},i}$ are, respectively, the number of events with $E_{\rm extra} = 0$ MeV, the number of events with $E_{\rm extra} > 30$ MeV, and the value of $E_{\rm extra}$ for the ith event.

The negative log likelihood is then minimized with respect to $N_{\rm sig}$ and $N_{\rm bkg}$ in the data sample. The resulting fitted values for $N_{\rm sig}$ and $N_{\rm bkg}$ are given in Table I. Figure 2 shows the $E_{\rm extra}$ distributions for $B^0 \to$ invisible and $B^0 \to$ invisible $+ \gamma$ with the fit superimposed.

The fitted signal yields are used to determine the decay branching fractions ($\mathcal{B}$), which are defined as

$$\mathcal{B} \equiv \frac{N_{\rm sig}}{\varepsilon \times N_{B\bar{B}}}, \quad (4)$$

TABLE I. Fitted yields of signal and background events in data. The uncertainties are statistical.

Mode	$N_{\rm sig}$	$N_{\rm bkg}$
$B^0 \to$ invisible	-22 ± 9	334 ± 21
$B^0 \to$ invisible $+ \gamma$	-3.1 ± 5.2	113 ± 12

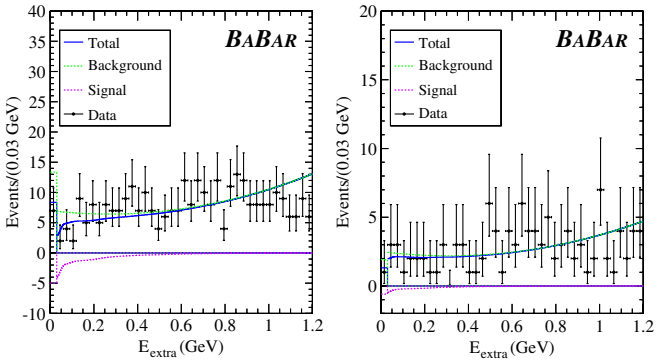

FIG. 2 (color online). Results of the maximum likelihood fit of E_{extra} for $B^0 \to$ invisible (left) and $B^0 \to$ invisible + γ (right).

where ε is the total signal efficiency, corrected for data-MC discrepancies (described below), and $N_{B\bar{B}}$ is the number of produced $B\bar{B}$ pairs.

The systematic uncertainty on the signal efficiency is dominated by data-MC discrepancies in the distribution of the variables used as input to the NN. This results in relative uncertainties of 6.1% and 8.2% for $B^0 \to$ invisible and $B^0 \to$ invisible + γ, respectively. This uncertainty is evaluated using the hypothesis that the data-MC agreement could reduce the discriminating power of each input variable. In order to make the signal distributions more backgroundlike, in the signal sample we apply a Gaussian smearing to each of the NN input variables, where the smearing parameters are evaluated by comparing the difference in the root mean square of the signal and background shapes. With this method correlations between variables are not considered but specific studies have indicated that the impact of the correlations is negligible. The NN output selection is then applied to this new sample and the difference between the nominal signal efficiency and this new efficiency is used as the systematic uncertainty.

Another important contribution is due to the estimation of the efficiency on the tag side reconstruction (3.5% for both channels). For this purpose, data and MC samples in which a B^0 and a $\bar{B}^0$ are both reconstructed as decays to $D^{(*)}\ell\nu$ in the same event ("double tag" events) are used. The square root of the ratio between the number of the selected double tag events in data and in MC simulation is 0.928 (0.824) for events with $B^0 \to D^{(*)}\ell\nu$ on the tag side; these ratios are used to correct the efficiency. The propagation of the statistical errors on the correction factors is used as a systematic uncertainty on the signal efficiency.

Other contributions to the systematic uncertainty on the signal efficiency come from the choice of the preselection criteria and from the SR definition of $m_D(\Delta m)$. The first effect is evaluated by applying a Gaussian smearing to the variables involved ($\cos\theta^*_{\text{miss}}$, $\cos\theta_{K\pi_1} + \cos\theta_{K\pi_2}$ and $\cos\theta_{\ell\pi_1} + \cos\theta_{\ell\pi_2}$). The variation on the signal efficiency is then used as a systematic uncertainty. As was done for the NN, this uncertainty is evaluated using the hypothesis that the discrimination power of each variable is reduced. The second effect is evaluated by changing each of the bounds of the SR definition by a value δ (3 MeV for m_D and 1.5 MeV for Δm), which is half of the $m_D/\Delta m$ resolution as evaluated in data. The relative maximum variation in efficiency is then used as a systematic uncertainty.

An additional source of systematic uncertainty is determined for the $B^0 \to$ invisible + γ decay in order to account for detector inefficiency in the single photon reconstruction. This is evaluated by comparing the data and MC π^0 reconstruction efficiency in $\tau \to \rho(\pi^\pm\pi^0)\nu$ decays, where the total number of produced π^0 in the selected sample is determined from the branching fraction of the specific τ decay [12]. Then the ratio between the two efficiencies, combined with the error on the τ decay branching ratio, is used to extract a systematic error for the single photon reconstruction efficiency.

The total systematic uncertainty on the signal selection efficiency is 7.7% for $B^0 \to$ invisible decay and 9.5% for $B^0 \to$ invisible + γ decay.

The systematic uncertainty on the number of signal events is dominated by the parametrization of the background E_{extra} distribution. A maximum likelihood fit of E_{extra} with the background parameters varied according to their statistical error and correlations is performed. For each parameter the difference in the fitted signal yield with respect to the nominal value is used as a systematic uncertainty. Other contributions to the signal yield systematic uncertainty come from the signal shape parametrization and from the use of the data SB for the determination of the background shape. The first is evaluated as the difference between the fitted yield with the polynomial shape and an alternative exponential shape. The latter, computed as the difference in the E_{extra} shape between the SR and SB, is

TABLE II. Summary of the systematic uncertainties.

Source	$B^0 \to$ invisible	$B^0 \to$ invisible + γ
Normalization errors		
B-counting	0.6%	0.6%
Efficiency errors		
Tagging efficiency	3.5%	3.5%
m_D (Δm) selection	1%	1.3%
Preselection	3%	2.4%
Neural network	6.1%	8.2%
Single photon	...	1.8%
Total	7.7%	9.5%
Yield errors (events)		
Background parameter	15.8	6.5
Signal parameter	2.0	1.2
Fit technique	...	1.0
E_{extra} shape	0.1	1.8
Total	15.9	6.9

parametrized with a first-order polynomial using the charge-conservation violating $B^+ \to$ invisible $(+\gamma)$ control sample discussed below. This parametrization is used to weight the background shape, and the difference in the fitted yield is used as a systematic uncertainty. Another contribution for the $B^0 \to$ invisible $+ \gamma$ decay is due to a small bias observed in MC studies of the yield extraction. The total systematic uncertainties on the signal yield are 16 and 7 events for $B^0 \to$ invisible and $B^0 \to$ invisible $+ \gamma$, respectively.

For the systematic contribution due to the uncertainty on the estimation of the total number of $B\bar{B}$ events in the data sample, the procedure adopted is described in Ref. [15] and the resulting uncertainty is 0.6%. The systematic uncertainties are summarized in Table II.

A Bayesian approach is used to set 90% confidence level (C.L.) upper limits on the branching fractions for $B^0 \to$ invisible and $B^0 \to$ invisible $+ \gamma$. Flat prior probabilities are assumed for positive values of both branching fractions. Gaussian likelihoods are adopted for signal yields. The Gaussian widths are fixed to the sum in quadrature of the statistical and systematic yield errors. We extract a posterior PDF using Bayes' theorem, including in the calculation the effect of systematic uncertainties associated with the efficiencies and the normalizations, modeled by Gaussian PDFs. Given the observed yields in Table I, the 90% C.L. upper limits are calculated, after the marginalization of the posterior PDF, by

$$\int_0^{UL} \mathcal{P}(\mathcal{B})d\mathcal{B} / \int_0^{\infty} \mathcal{P}(\mathcal{B})d\mathcal{B} = 0.9. \qquad (5)$$

The resulting upper limits on the branching fractions are

$$\mathcal{B}(B^0 \to \text{invisible}) < 2.4 \times 10^{-5},$$
$$\mathcal{B}(B^0 \to \text{invisible} + \gamma) < 1.7 \times 10^{-5}$$

at 90% C.L. In order to cross-check the results of the analysis, we also search for the charge-conservation violating modes $B^+ \to$ invisible and $B^+ \to$ invisible $+ \gamma$. We check that their resulting signal is consistent with zero. For these modes, we reconstruct $B^{\pm} \to D^0 \ell \nu X^0$, where X^0 can be a photon, π^0, or nothing. The D^0 is reconstructed in the same three decay modes as in $B^0 \to D^{(*)-} \ell^+ \nu$, and similar criteria are enforced for the reconstructed charged B as for the neutral B modes. The resulting fitted values of $N_{\rm sig}$ are -4.3 ± 3.8 (stat.) for $B^+ \to$ invisible and -7.9 ± 8.3 (stat.) for $B^+ \to$ invisible $+ \gamma$, which are both consistent with zero within 1.1 standard deviations.

In summary, we obtain improved limits on branching fractions for B^0 decays to an invisible final state and for B^0 decays to invisible $+\gamma$. The upper limits at 90% C.L. are 2.4×10^{-5} and 1.7×10^{-5} for the $B^0 \to$ invisible and $B^0 \to$ invisible $+ \gamma$ branching fractions, respectively. The latter limit assumes a photon momentum distribution predicted by the constituent quark model for $B^0 \to \nu\bar{\nu}\gamma$ decay [4], whereas the $B^0 \to$ invisible limit is not decay-model dependent. These limits supersede our earlier results [2], which used a small fraction of our present data set.

We are grateful for the excellent luminosity and machine conditions provided by our PEP-II colleagues, and for the substantial dedicated effort from the computing organizations that support *BABAR*. The collaborating institutions wish to thank SLAC for its support and kind hospitality. This work is supported by DOE and NSF (USA), NSERC (Canada), CEA and CNRS-IN2P3 (France), BMBF and DFG (Germany), INFN (Italy), FOM (The Netherlands), NFR (Norway), MES (Russia), MICIIN (Spain), and STFC (United Kingdom). Individuals have received support from the Marie Curie EIF (European Union) and the A. P. Sloan Foundation (USA).

[1] Charge-conjugate decay modes are implied throughout this paper.
[2] B. Aubert *et al.* (*BABAR* Collaboration), Phys. Rev. Lett. **93**, 091802 (2004).
[3] G. Buchalla and A. J. Buras, Nucl. Phys. **B400**, 225 (1993).
[4] C. D. Lu and D. X. Zhang, Phys. Lett. B **381**, 348 (1996).
[5] T. Adams *et al.* (NuTeV Collaboration), Phys. Rev. Lett. **87**, 041801 (2001).
[6] A. Dedes, H. Dreiner, and P. Richardson, Phys. Rev. D **65**, 015001 (2001).
[7] K. Agashe, N. G. Deshpande, and G.-H. Wu, Phys. Lett. B **489**, 367 (2000).
[8] K. Agashe and G.-H. Wu, Phys. Lett. B **498**, 230 (2001).
[9] H. Davoudiasl, P. Langacker, and M. Perelstein, Phys. Rev. D **65**, 105015 (2002).
[10] B. Aubert *et al.* (*BABAR* Collaboration), Nucl. Instrum. Methods Phys. Res., Sect. A **479**, 1 (2002).
[11] S. Agostinelli *et al.* (GEANT4 Collaboration), Nucl. Instrum. Methods Phys. Res., Sect. A **506**, 250 (2003).
[12] K. Nakamura *et al.* (Particle Data Group), J. Phys. G **37**, 075021 (2010).
[13] A. Hoecker *et al.*, Proc. Sci., ACAT2007 (2007) 040.
[14] K. S. Cranmer, Comput. Phys. Commun. **136**, 198 (2001).
[15] G. D. McGregor, arXiv:0812.1954.